HHS Public Access

Author manuscript

ACS Chem Biol. Author manuscript; available in PMC 2018 February 17.

Published in final edited form as:

ACS Chem Biol. 2017 February 17; 12(2): 407–413. doi:10.1021/acschembio.6b00981.

A rationally-designed, general strategy for membrane orientation of photoinduced electron transfer-based voltage-sensitive dyes

Rishikesh U. Kulkarni[†], **Hang Yin**[‡], **Narges Pourmandi**[†], **Feroz James**[†], **Maroof M. Adil**[|], **David V. Schaffer**[|,||], **Yi Wang**[‡,*], and **Evan W. Miller**[†,§,||,*]

[†]Department of Chemistry, University of California, Berkeley, CA 94720

[§]Department of Molecular and Cell Biology, University of California, Berkeley, CA 94720

[|]Department of Chemical and Biomolecular Engineering, University of California, Berkeley, CA 94720

[||]Helen Wills Neuroscience Institute, University of California, Berkeley, CA 94720

[‡]Shenzhen Research Institute and Department of Physics, Chinese University of Hong Kong, Shatin, N.T., Hong Kong

Abstract

Voltage imaging with fluorescent dyes offers promise for interrogating the complex roles of membrane potential in coordinating the activity of neurons in the brain. Yet, low sensitivity often limits the broad applicability of optical voltage indicators. In this paper, we use molecular dynamics (MD) simulations to guide the design of new, ultra-sensitive fluorescent voltage indicators that use photoinduced electron transfer (PeT) as a voltage-sensing switch. MD simulations predict an approximately 16% increase in voltage sensitivity resulting purely from improved alignment of dye with the membrane. We confirm this theoretical finding by synthesizing 9 new voltage-sensitive (VoltageFluor, or VF) dyes and establishing that all of them display the expected improvement of approximately 19%. This synergistic outworking of theory and experiment enabled computational and theoretical estimation of VF dye orientation in lipid bilayers and has yielded the most sensitive PeT-based VF dye to date. We use this new voltage indicator to monitor voltage spikes in neurons from rat hippocampus and human pluripotent stem cell-derived dopaminergic neurons.

Graphical abstract

[*]Corresponding Author: evanwmiller@berkeley.edu, yiwang@phy.cuhk.edu.hk.

Supporting Information.

Synthetic details, spectroscopic analysis, supplemental cell imaging data, computational parameters, and molecular dynamics simulation movie files.

This paper contains enhanced objects.

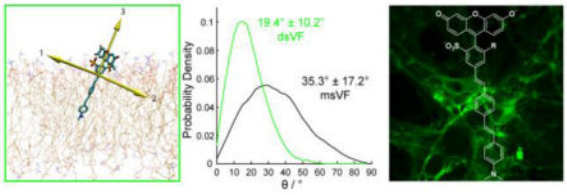

The development of fluorescent indicators for biological analytes has revolutionized our ability to interrogate biochemistry and biophysics in living cells. However, the design of fluorescent dyes and sensors remains an outstanding challenge in the field.(1–12) Our group has recently initiated a program to build new chemical indicators for sensing membrane potential,(13–15) in order to further understand the roles that membrane voltage plays, not only in excitable cells, such as neurons and cardiomyocytes, but also in non-excitable cells in the rest of the body. Traditional methods to measure membrane potential rely on invasive electrodes, introduced via pipette or on micro or nano-arrays. Voltage imaging with fluorescent indicators, whether genetically-encoded(16) or chemically synthesized,(15) is an attractive solution because such imaging circumvents problems of low-throughput, low spatial resolution, and high invasiveness associated with more traditional electrode-based techniques.(17–19) Our lab is developing VoltageFluor, or VF, dyes which are a small molecule platform for voltage imaging operating via a photoinduced electron transfer (PeT) quenching mechanism(20, 21) to directly image transmembrane voltage changes.(13, 14, 22, 23) Previously reported VF dyes have proven useful for measuring membrane potential in a number of biological contexts ranging from isolated synaptic vesicles(24) to intact leech neuronal ganglia(25, 26) to stem cell-derived cardiomyocytes,(27, 28) among others.(29, 30) Improvement of genetically-encoded voltage indicators relies on site-directed mutagenesis and large-scale screening,(16) while small-molecule voltage indicators have the potential for rational improvement. However, a comprehensive design scheme for VF dyes remains elusive, due in part to our incomplete understanding of the biophysical properties influencing voltage sensitivity in the VoltageFluor scaffolds.

We therefore desired to study and improve a single, key aspect of the PeT-quenching mechanism(21) of VF dyes. We propose that VF dyes sense voltage via a PeT-based mechanism where the transmembrane potential of the cell strongly influences the rate of PeT: at hyperpolarizing, or negative, potentials, PeT is accelerated and fluorescence is quenched. At depolarizing, or positive, voltages, fluorescence increases as the rate of PeT decreases. Pioneering work by Loew and co-workers modeled the voltage sensitivity of electrochromic voltage-sensitive dyes and proposed that the magnitude of the molecular Stark effect, or perturbation of the chromophore orbital energies, which gives rise to the voltage sensitivity of these compounds, is proportional to the following expression:(31, 32)

$$\Delta F/F \propto \Delta G = q\vec{r} \cdot \vec{E} \quad \text{Equation 1}$$

Where ΔF/F is the fractional voltage sensitivity of a dye, ΔG represents the change in energy associated with the shift in wavelength, q is the effective charge transferred, $\vec{r}$ is the distance

that quantity q travels and $\vec{E}$ is the electric field. By extension to PeT-based voltage sensitive dyes, the voltage sensitivity should be proportional to the change in driving force for PeT, which may be modeled by a similar equation when the transmembrane potential is within a physiologically-relevant range.(21) Because the interaction between the transferred electron and the membrane potential is highest when the electron transfer vector and electric field vectors are aligned and at a minimum when perpendicular, equation (1) can be rewritten as

$$\Delta F/F \propto \Delta G = qrE\cos\theta \quad \text{Equation 2}$$

where θ is the angle of displacement, or tilt, between the electron transfer vector and the electric field vector (Figure 1a–c).

Our initial assumption was that the tilt angle θ was close to 0°, thus giving us the maximum voltage sensitivity for a given dye, where q, r, and E remain constant. To test this hypothesis, ascertain how VF dyes orient in the membrane, and propose new structural motifs for voltage sensing, we turned to molecular modeling to measure the tilt angle of VF2.1.Cl, a prototypical VF dye, in a simulated lipid bilayer.

RESULTS AND DISCUSSION

We parameterized VF2.1.Cl with the CHARMM general force field (33) (see SI Fig. 1 and SI Text for details) and then performed molecular dynamics (MD) simulations of the VF dye embedded in a 1-palmitoyl-2-oleoyl-*sn*-glycerol-3-phosphocholine (POPC) lipid bilayer, as a simplified model of a mammalian cell membrane.(34, 35) By modeling the behavior of VF2.1.Cl in a POPC lipid bilayer, we aimed to both make observations regarding the tilt angle and propose structural modifications that we could then synthesize to assess changes in voltage sensitivity. We performed three replicates of ~500 ns molecular dynamics simulations of VF2.1.Cl in a pure POPC membrane and sampled the tilt angle θ (between the long axis of VF and the membrane normal) every 5 ps via principal component analysis (PCA). As shown in Figure 1d (SI Movie 1), the 2′ sulfonate of VF2.1.Cl localized primarily at the lipid:water interface, presumably to avoid burying the charged sulfonate in the non-polar lipid groups. Because the sulfonate of VF2.1.Cl is unsymmetrically positioned off the main axis of VF2.1.Cl, this results in a considerable tilt, with an average angle of 35° (Fig. 1d and f, **Web Enhanced Object 1**). Furthermore, the molecule appeared to be rather “floppy” in the membrane, with a standard deviation in the tilt angle of 17° (Fig. 1f) and a correlation time of 9.7 ns (±2.6 ns, ±SEM, n=3 simulations) (SI Fig. 2). An average tilt angle of 35° implies that the voltage sensitivity of VF2.1.Cl is only about 82% (cosine of 35°) of the theoretical maximum, assuming q and r remain the same. We wondered whether “straightening” VF dyes in the membrane would prove a general method for enhancing voltage sensitivity by approximately 22% (1/cosine 35°).

We reasoned that the tilt angle of the VF dye could be reduced in a straightforward manner by adding a second sulfonate group in the *ortho*-position on the meso-aryl ring of the xanthene chromophore (Fig. 1a–c). We hoped the new, doubly-sulfonated, disulfoVF dyes (dsVF), with two opposing sulfonate groups at the 2′- and 6′-positions, would have both

reduced overall tilt angle and increased rigidity since exposing one sulfonate to bulk water via tilting the whole molecule would require the other sulfonate to become buried in the non-polar lipid layer. Overall, we hypothesized that smaller fluctuations in the tilt angle of dsVF would cause an improvement in voltage sensitivity relative to monosulfoVF dyes (msVF).

We used MD simulations to test whether the proposed dsVF dye displays enhanced alignment within a model membrane relative to its monosulfo counterpart. MD simulations of dsVF2.1.Cl (Fig. 1d–e, **Web Enhanced Object 2**) reveal a significant reduction in the tilt angle, θ, compared to msVF2.1.Cl: 19°±10° for dsVF2.1.Cl and 35°±17° for msVF2.1.Cl (Fig. 1f). Compared to msVF, dsVF displays less conformational flexibility within the lipid bilayer, as reflected in the smaller standard deviation of θ values for dsVF2.1.Cl (10° for dsVF vs. 17 ° for msVF). Analysis of the correlation time for msVF2.1.Cl reveals a much longer periodicity in θ fluctuations (9.7±2.6 ns; ±SEM, n = 3 simulations) with larger magnitude swings away from the average orientation (SI Fig. 2). In contrast, dsVF2.1.Cl has a much shorter period (1.8±0.1 ns; ±SEM, n= 3 simulations) characterized by smaller fluctuations in the average angle of displacement (SI Fig. 1b)

The increased rigidity of the dsVF dye comes primarily from a restriction in the movement of the dye in a single plane. Molecular orientation in the plane of the sulfonates (defined as the angle between the vector parallel to the meso ring system, “ArylP,” and the membrane normal “Z” (Fig. 2a) becomes more rigid upon going from msVF (61.3°) to dsVF (92.8°) (Fig. 2b–d). In contrast, motion in the plane perpendicular to the sulfonates (defined as the angle between the vector normal to the meso ring system, “ArylN” and the membrane normal, Fig. 2a) is relatively unchanged, shifting from 88.3° for msVF2.1.Cl to 92.0° for dsVF2.1.Cl (Fig. 2b–c and e). This is consistent with the hypothesis that symmetric sulfonation rigidifies VF dyes in the plane parallel to the meso aromatic ring, ArylP, but has little effect on motion in the orthogonal coordinate, ArylN (Fig. 2b–c).

Based on the MD simulations, we estimate an approximate 16% increase in voltage sensitivity upon going from a msVF to dsVF dye scaffold, if molecular orientation, or θ, is the only change. This improvement represents a critical increase in the sensitivity of VF-type dyes. According to Equation 3, for a given msVF/dsVF pair, the change in voltage sensitivity should be proportional to the ratio between the cosine of θ for msVF and dsVF.

$$\frac{\Delta F/F_{dsVF}}{\Delta F/F_{msVF}} \propto \frac{cos\,\theta_{dsVF}}{cos\,\theta_{msVF}} \quad \text{Equation 3}$$

Therefore, a change in θ from 35.4° to 19.4° should give a 16% increase in voltage sensitivity (cosine of 19.4°/cosine of 35.4° = 1.157).

To confirm the MD simulation results and experimentally test the hypothesis that improved orientation produces an increase in voltage sensitivity, we synthesized and characterized 6 new doubly-sulfonated VF dyes. Although the chromophores required for msVF are accessible via sulfonic acid anhydrides,(36) generation of the doubly-sulfonated precursors

represented a synthetic challenge. To circumvent this problem, we devised a route from commercially available fluorobenzaldehydes (**1** and **2**) that enabled access to both singly and doubly sulfonated dye precursors. Sulfonated halobenzaldehydes **3** and **4** could be prepared via nucleophilic aromatic substitution (S_NAr) with sodium sulfite/bisulfite,(37) enabling us to bypass both the deactivating nature of the sulfonate group and any challenges in directing the sulfonate substitution pattern. Both 5-bromo-2-formyl-benzenesulfonic acid **3** and 5-bromo-2-formyl-1,3-benzenedisulfonic acid **4** were prepared in good yields (72–76%) on the gram scale from commercially available 4-bromo-mono- and di-fluorobenzaldehydes via S_NAr with sodium sulfite/bisulfite in a mixture of water and ethanol.

These aldehydes then condensed smoothly with unsubstituted and halogenated resorcinols in methanesulfonic acid (with *in situ* oxidation by air) to give an array of monosulfonated and disulfonated fluoresceins (**5-10**), with yields ranging from 40–84% (Figure 3). Generally, yields of monosulfo-fluoresceins (70–84%) were higher than for corresponding disulfo-fluoresceins (40–55%), which we attribute to the increased steric congestion of disulfo- vs. monosulfobenzaldehydes. The new disulfo-fluoresceins show absorption and emission profiles similar to their mono-sulfo counterparts and display high fluorescence quantum yields (near unity, SI Fig. 3) and aqueous solubility: up to 0.94 mM in H_2O with 0.1% DMSO for ds-dichlorofluorescein vs. only 0.41 mM for ms-dichlorofluorescein.

Methoxy-substituted anilines generally give the best voltage sensitivity in the context of a fluorescein-based voltage sensor,(23) so we sought to make both 3-methoxy and unsubstituted aniline molecular wires to test if straightening via double sulfonation is a generalizable strategy. We used either a dimethyl aniline molecule wire or a N,N-diethyl-3-methoxyaniline wire as the two molecular wire scaffolds in this study. The N,N-diethyl-3-methoxyaniline was used in place of the previously described N,N-dimethyl-3-methoxyaniline wire because the diethyl derivative can be simply prepared from commercially available N,N-diethylsalicylaldehyde.(38) Heck coupling between the styrene molecular wires and corresponding mono- or di-sulfonated fluoresceins provided the ms- and dsVF dyes after purification via crystallization. Small amounts of dye were purified by semi-preparative HPLC for further analysis.

We synthesized a total of 9 new dyes: 6 new dsVF dyes and 3 new msVF dyes. Both msVF and dsVF dyes display similar excitation and emission profiles to previously reported msVF dyes (Table 1, SI Fig. 4), and all localized to the plasma membrane when applied to HEK293T cells via bath loading. (Fig. 3a–b, SI Fig. 5). In general, disulfonated fluorophores (**8-10**) and dsVF dyes (**11b-16b**) showed improved aqueous solubility relative to mono-sulfo derivatives (**5-7, 11a-16a**). Addition of a second sulfonate improved the aqueous solubility of fluorophore **8** 2.3-fold relative to monosulfo **5**, as determined either spectroscopically or gravimetrically (SI text). In the context of a full VF dye, a second sulfonate improved aqueous solubility by 22% for VF2.1.Cl and 55% for VF2.2(OMe).Cl (**11a** vs **11b; 12a** vs **12b;** SI Fig. 6).

To determine the voltage sensitivity of each of the dyes, we performed whole-cell patch clamp electrophysiology on HEK293T cells loaded with 200 nM VF (Fig. 3a–d). Depolarization of the cell membrane in the presence of VF dye results in a large increase of

fluorescence, while hyperpolarization results in lower levels of fluorescence (Fig. 3c–d; SI Fig. 7). As a illustrative comparison, we found that msVF2.2(OMe).Cl (**12a**) had a voltage sensitivity of approximately 53% ± 1% ΔF/F per 100 mV, which is comparable to the previously reported msVF2.1(OMe).Cl, at 48% per 100 mV.(23) The disul foVF2.2(OMe).Cl (**12b**), when subjected to the same membrane depolarizations, had a voltage sensitivity of 63% ± 1% ΔF/F per 100 mV, representing a 19% improvement in voltage sensitivity over the monosulfonated VF analog, and the most sensitive VF dye to date.

We determined the voltage sensitivity for the remaining 10 VF dyes using dual optical and electrophysiological recordings in HEK cells (3–8 separate cells per dye). All of the dyes—VF2.1.Cl (**11**), VF2.1.H (**13**), VF2.1.F (**15**), VF2.2(OMe).H (**14**), and VF2.2(OMe).F (**16**)—showed comparable improvements in voltage sensitivity when the second sulfonate group is added (Table 1, Fig 4.). In all cases, we see an increase in voltage sensitivity upon transition to the dsVF dye. On average di-sulfoVF dyes show a 19% ± 2% increase in voltage sensitivity over its monosulfonated counterpart (Table 1). The experimentally determined average increase in voltage sensitivity of 19% matches well with the computationally predicted value of 16% and provides a validation both of our MD simulation methodology and our hypothesis that the relative orientation of the VF dye influences voltage sensitivity. The small discrepancy may arise from differences in the electronic nature of ms- vs dsVF dyes, which is known to affect voltage sensitivity.(23)

Due to its exceptional voltage sensitivity and good photostability compared to msVF2.2(OMe).Cl (SI Figure 8), we expected that disulfoVF2.2(OMe).Cl should be well-suited to observing membrane potential changes in neurons. Cultured rat hippocampal neurons bathed in disulfoVF2.2(OMe).Cl showed bright membrane staining, as confirmed by confocal microscopy (Fig. 5a). We also used dsVF2.2(OMe).Cl to image neuronal activity in midbrain dopaminergic (mDA) neurons derived from cultured human pluripotent stem cells (hPSCs) in culture (Fig. 5b) using differentiation conditions adapted from previously established protocols.(39) mDA neurons stained with dsVF2.2(OMe).Cl revealed distinct firing patterns (Fig. 5c, d). Functional analysis of human- or patient-derived differentiated neurons in a simple, non-invasive manner enabled by dsVF2.2(OMe).Cl may be an important diagnostic tool alongside more conventional methods in ascertaining proper differentiation as well as in investigating human disease phenotypes.

CONCLUSIONS

In summary, we use a molecular modeling approach to study the effects of dye orientation within the plasma membrane on the voltage sensitivity of VoltageFluor dyes and use the model to propose the structure of a dye with enhanced voltage sensitivity over previous incarnations of VF dyes. Based on orientation effects observed in MD simulations, we predicted an approximate 16% increase in the voltage sensitivity of dsVF dyes.

To validate our computational results, we present the design and synthesis of disulfonated fluoresceins, a novel group of xanthene fluorophores with increased water solubility. The new disulfonated xanthene fluorophores may be useful in their own right as labeling agents

due to their ease of synthesis in isomerically-pure form, high water solubility, and potential for derivatization. We then synthesize new, more rigid disulfo-VoltageFluor dyes based on these novel disulfonated fluoresceins. All of the dsVF dyes display enhanced voltage sensitivity relative to their msVF cognates, with an average increase in sensitivity of 19%, which matches well with our calculated improvement of 16%.

These results validate our hypothesis that proper orientation of a VF dye within the membrane significantly influences its voltage sensitivity, in addition to providing excellent support for a PeT-based mechanism of voltage sensitivity. One of the new VF dyes, disulfoVF2.2(OMe).Cl shows the highest voltage sensitivity observed in PeT-based voltage sensors thus far (63% ΔF/F per 100 mV). Additionally, we demonstrate that disulfoVF2.2(OMe).Cl can be used to detect membrane potential changes in rat hippocampal neurons and in human-derived midbrain dopaminergic neurons.

The improved voltage sensitivity of disulfoVF2.2(OMe).Cl facilitates voltage imaging under conditions that degrade signal-to-noise ratio and sensitivity, such as low-power illumination, thicker tissue samples, and long-term imaging. Finally, the disulfonated VoltageFluor dyes represent one possible solution for designing future dyes with higher voltage sensitivity than first generation VF dyes. Efforts are currently underway in our lab to generalize this scaffold to other xanthene chromophores, such as rhodamines(38) and silicon-rhodamines(13), and integrate it with our understanding of the contributions electron affinities make to voltage sensing(23).

Supplementary Material

Refer to Web version on PubMed Central for supplementary material.

Acknowledgments

EWM acknowledges generous support from the University of California, Berkeley, Hellman Foundation, Alzheimer's Association (2016-NIRG-394290), March of Dimes (5-FY16-65), Sloan Foundation, Klingenstein-Simons Foundation, and the National Institute of Neurological Disorders and Stroke (R00 NS07581), and the National Institute for General Medical Sciences (R35 GM119855). RUK was supported in part by a Chemical Biology Training grant from the National Institute of General Medical Sciences (T32 GM066698). MMA was supported in part by CIRM Training Grant TG2-01164 and CIRM RT3-07800. YW acknowledges project 21403183 supported by the NSFC and the Special Program for Applied Research on Super Computation of the NSFC-Guangdong Joint Fund (the second phase). Funds for the QB3 900 MHz NMR Spectrometer were provided by the NIH through grant GM68933. We dedicate this manuscript to the memory of our late colleague, Professor Roger Y. Tsien.

References

1. Grimm JB, English BP, Chen JJ, Slaughter JP, Zhang ZJ, Revyakin A, Patel R, Macklin JJ, Normanno D, Singer RH, Lionnet T, Lavis LD. A general method to improve fluorophores for live-cell and single-molecule microscopy. Nat Methods. 2015; 12:244. [PubMed: 25599551]
2. Lavis LD, Raines RT. Bright Building Blocks for Chemical Biology. Acs Chem Biol. 2014; 9:855–866. [PubMed: 24579725]
3. Kushida Y, Nagano T, Hanaoka K. Silicon-substituted xanthene dyes and their applications in bioimaging. Analyst. 2015; 140:685–695. [PubMed: 25380094]
4. Brewer TF, Chang CJ. An Aza-Cope Reactivity-Based Fluorescent Probe for Imaging Formaldehyde in Living Cells. J Am Chem Soc. 2015; 137:10886–10889. [PubMed: 26306005]

5. Aron AT, Ramos-Torres KM, Cotruvo JA, Chang CJ. Recognition- and Reactivity-Based Fluorescent Probes for Studying Transition Metal Signaling in Living Systems. Accounts Chem Res. 2015; 48:2434–2442.
6. Kobayashi H, Ogawa M, Alford R, Choyke PL, Urano Y. New Strategies for Fluorescent Probe Design in Medical Diagnostic Imaging. Chem Rev. 2010; 110:2620–2640. [PubMed: 20000749]
7. Lee HLD, Lord SJ, Iwanaga S, Zhan K, Xie HX, Williams JC, Wang H, Bowman GR, Goley ED, Shapiro L, Twieg RJ, Rao JH, Moerner WE. Superresolution Imaging of Targeted Proteins in Fixed and Living Cells Using Photoactivatable Organic Fluorophores. J Am Chem Soc. 2010; 132:15099–15101. [PubMed: 20936809]
8. Anzalone AV, Wang TY, Chen ZX, Cornish VW. A Common Diaryl Ether Intermediate for the Gram-Scale Synthesis of Oxazine and Xanthene Fluorophores. Angew Chem Int Edit. 2013; 52:650–654.
9. Yun SW, Kang NY, Park SJ, Ha HH, Kim YK, Lee JS, Chang YT. Diversity Oriented Fluorescence Library Approach (DOFLA) for Live Cell Imaging Probe Development. Accounts Chem Res. 2014; 47:1277–1286.
10. Lukinavicius G, Umezawa K, Olivier N, Honigmann A, Yang GY, Plass T, Mueller V, Reymond L, Correa IR, Luo ZG, Schultz C, Lemke EA, Heppenstall P, Eggeling C, Manley S, Johnsson K. A near-infrared fluorophore for live-cell super-resolution microscopy of cellular proteins. Nat Chem. 2013; 5:132–139. [PubMed: 23344448]
11. Uno SN, Kamiya M, Yoshihara T, Sugawara K, Okabe K, Tarhan MC, Fujita H, Funatsu T, Okada Y, Tobita S, Urano Y. A spontaneously blinking fluorophore based on intramolecular spirocyclization for live-cell super-resolution imaging. Nat Chem. 2014; 6:681–689. [PubMed: 25054937]
12. Lincoln R, Greene LE, Krumova K, Ding ZT, Cosa G. Electronic Excited State Redox Properties for BODIPY Dyes Predicted from Hammett Constants: Estimating the Driving Force of Photoinduced Electron Transfer. J Phys Chem A. 2014; 118:10622–10630. [PubMed: 25066755]
13. Huang YL, Walker AS, Miller EW. A Photostable Silicon Rhodamine Platform for Optical Voltage Sensing. J Am Chem Soc. 2015; 137:10767–10776. [PubMed: 26237573]
14. Grenier V, Walker AS, Miller EW. A Small-Molecule Photoactivatable Optical Sensor of Transmembrane Potential. J Am Chem Soc. 2015; 137:10894–10897. [PubMed: 26247778]
15. Miller EW. Small molecule fluorescent voltage indicators for studying membrane potential. Curr Opin Chem Biol. 2016; 33:74–80. [PubMed: 27318561]
16. Yang HH, St-Pierre F. Genetically Encoded Voltage Indicators: Opportunities and Challenges. The Journal of Neuroscience. 2016; 36:9977–9989. [PubMed: 27683896]
17. Peterka DS, Takahashi H, Yuste R. Imaging voltage in neurons. Neuron. 2011; 69:9–21. [PubMed: 21220095]
18. Scanziani M, Hausser M. Electrophysiology in the age of light. Nature. 2009; 461:930–939. [PubMed: 19829373]
19. Braubach O, Cohen LB, Choi Y. Historical Overview and General Methods of Membrane Potential Imaging. Adv Exp Med Biol. 2015; 859:3–26. [PubMed: 26238047]
20. De Silva AP, Gunaratne HQN, Habibjiwan JL, Mccoy CP, Rice TE, Soumillion JP. New Fluorescent Model Compounds for the Study of Photoinduced Electron-Transfer - the Influence of a Molecular Electric-Field in the Excited-State. Angew Chem Int Edit. 1995; 34:1728–1731.
21. Li LS. Fluorescence probes for membrane potentials based on mesoscopic electron transfer. Nano Lett. 2007; 7:2981–2986. [PubMed: 17880257]
22. Miller EW, Lin JY, Frady EP, Steinbach PA, Kristan WB Jr, Tsien RY. Optically monitoring voltage in neurons by photo-induced electron transfer through molecular wires. Proc Natl Acad Sci U S A. 2012; 109:2114–2119. [PubMed: 22308458]
23. Woodford CR, Frady EP, Smith RS, Morey B, Canzi G, Palida SF, Araneda RC, Kristan WB Jr, Kubiak CP, Miller EW, Tsien RY. Improved PeT molecules for optically sensing voltage in neurons. J Am Chem Soc. 2015; 137:1817–1824. [PubMed: 25584688]
24. Farsi Z, Preobraschenski J, van den Bogaart G, Riedel D, Jahn R, Woehler A. Single-vesicle imaging reveals different transport mechanisms between glutamatergic and GABAergic vesicles. Science. 2016; 351:981–984. [PubMed: 26912364]

25. Wagenaar DA. A classic model animal in the 21st century: recent lessons from the leech nervous system. J Exp Biol. 2015; 218:3353–3359. [PubMed: 26538172]
26. Frady EP, Kapoor A, Horvitz E, Kristan WB Jr. Scalable Semisupervised Functional Neurocartography Reveals Canonical Neurons in Behavioral Networks. Neural Comput. 2016; 28:1453–1497. [PubMed: 27348420]
27. Asakura K, Hayashi S, Ojima A, Taniguchi T, Miyamoto N, Nakamori C, Nagasawa C, Kitamura T, Osada T, Honda Y, Kasai C, Ando H, Kanda Y, Sekino Y, Sawada K. Improvement of acquisition and analysis methods in multi-electrode array experiments with iPS cell-derived cardiomyocytes. J Pharmacol Tox Met. 2015; 75:17–26.
28. Dempsey, GT., Chaudhary, KW., Atwater, N., Nguyen, C., Brown, BS., McNeish, JD., Cohen, AE., Kralj, JM. Cardiotoxicity screening with simultaneous optogenetic pacing, voltage imaging and calcium imaging. J Pharmacol Tox Met. 2016. doi.org/10.1016/j.vascn.2016.1005.1003
29. Ceriani F, Mammano F. A rapid and sensitive assay of intercellular coupling by voltage imaging of gap junction networks. Cell Commun Signal. 2013; 11doi: 10.1186/1478-1811X-1111-1178
30. Dolensek J, Stozer A, Klemen MS, Miller EW, Rupnik MS. The Relationship between Membrane Potential and Calcium Dynamics in Glucose-Stimulated Beta Cell Syncytium in Acute Mouse Pancreas Tissue Slices. Plos One. 2013; 8doi: 10.1371/journal.pone.0082374
31. Loew LM, Bonneville GW, Surow J. Charge Shift Optical Probes of Membrane-Potential - Theory. Biochemistry-Us. 1978; 17:4065–4071.
32. Loew, LM. Design and Use of Organic Voltage Sensitive Dyes. In: Canepari, M.Zecevic, D., Bernus, O., editors. Adv Exp Med Biol. Springer-Verlag; Berlin, Berlin: 2015. p. 27-53.
33. Vanommeslaeghe K, Hatcher E, Acharya C, Kundu S, Zhong S, Shim J, Darian E, Guvench O, Lopes P, Vorobyov I, MacKerell AD. CHARMM General Force Field: A Force Field for Drug-Like Molecules Compatible with the CHARMM All-Atom Additive Biological Force Fields. J Comput Chem. 2010; 31:671–690. [PubMed: 19575467]
34. Hong C, Tieleman DP, Wang Y. Microsecond Molecular Dynamics Simulations of Lipid Mixing. Langmuir. 2014; 30:11993–12001. [PubMed: 25237736]
35. van Meer G, Voelker DR, Feigenson GW. Membrane lipids: where they are and how they behave. Nat Rev Mol Cell Bio. 2008; 9:112–124. [PubMed: 18216768]
36. Jiao GS, Han JW, Burgess K. Syntheses of regioisomerically pure 5-or 6-halogenated fluoresceins. J Org Chem. 2003; 68:8264–8267. [PubMed: 14535816]
37. Kovi, R., Nampalli, S., Tharial, PX. Chemical Indexing Equivalent to 149:533918 (WO). Apicore, LLC; USA: 2008. Process for preparation and purification of isosulfan blue; p. 7
38. Deal PE, Kulkarni RU, Al-Abdullatif SH, Miller EW. Isomerically Pure Tetramethylrhodamine Voltage Reporters. J Am Chem Soc. 2016; 138:9085–9088. [PubMed: 27428174]
39. Kriks S, Shim JW, Piao JH, Ganat YM, Wakeman DR, Xie Z, Carrillo-Reid L, Auyeung G, Antonacci C, Buch A, Yang LC, Beal MF, Surmeier DJ, Kordower JH, Tabar V, Studer L. Dopamine neurons derived from human ES cells efficiently engraft in animal models of Parkinson's disease. Nature. 2011; 480:547–U177. [PubMed: 22056989]

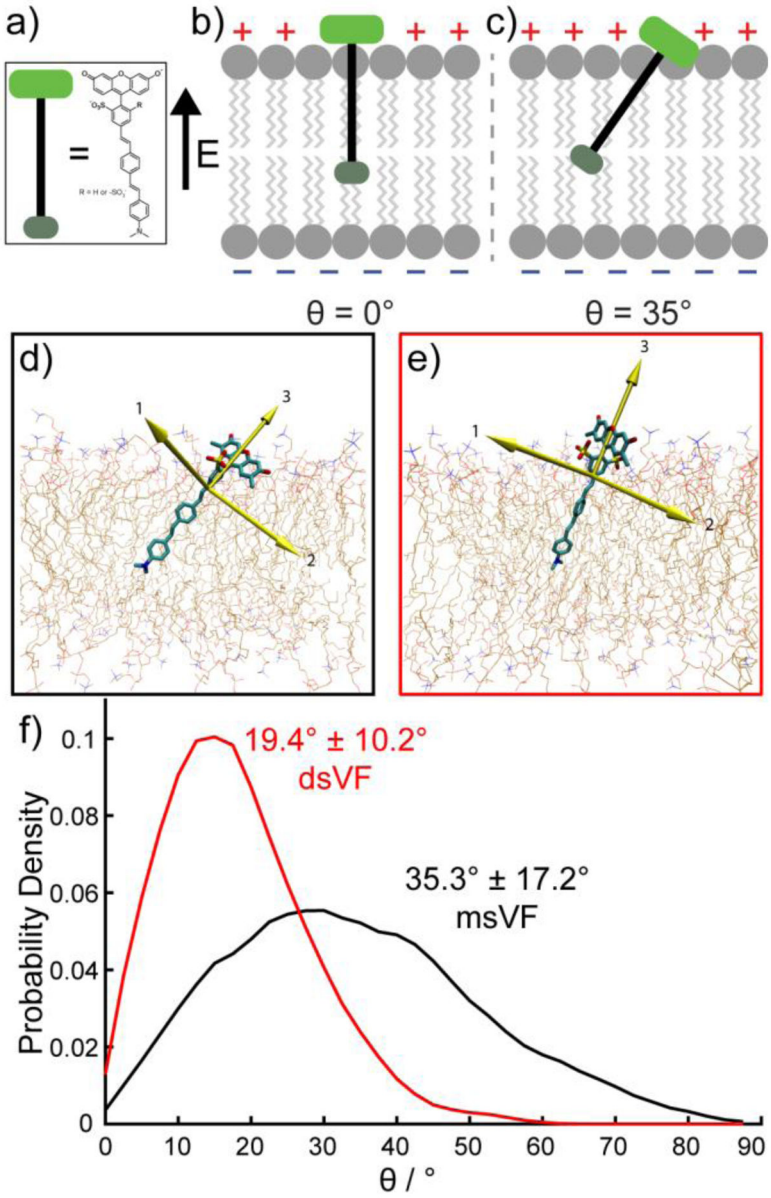

Figure 1.

Orientation of ms and ds VF dyes. Schematic representation of a)VF dye alignment in the plasma membrane. b) Maximum voltage sensitivity is predicted when theta = 0° (left) and is lowest when theta = 90° (not shown). c) Intermediate values of theta (right) reduce voltage sensitivity. Snapshots of MD simulations in POPC lipid bilayers show d) msVF and e) dsVF. Yellow arrows indicate principal components. f) Plot of probability density vs. angle of displacement between the 3rd principle component (the long axis) of VF dyes and the membrane normal.

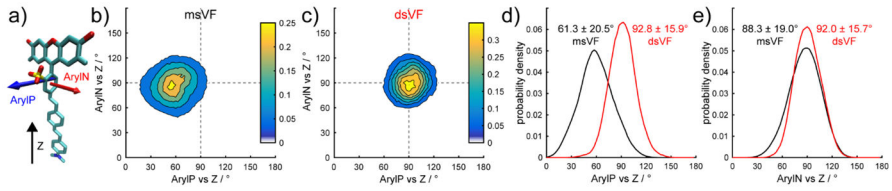

Figure 2.

Calculated orientation of msVF and dsVF in a POPC lipid bilayer. a) Definition of vectors used to examine angles in VF dyes. “ArylP” describes the vector parallel to the *meso*-aryl ring; “ArylN” describes the vector normal to the plane of the aryl ring; and “Z” is the membrane normal. Contour plots describe the the ArylP vs Z and ArylN vs Z dihedral angles for a given snapshot of the simulation for b) msVF and c) dsVF. The dotted lines serve as a visual guide for a perfect 90° orientation between the dye and the membrane normal. The distribution of dihedral angles sampled during a simulation for d) ArylP vs Z and e) ArylN vs Z are plotted for both msVF (black) and dsVF (red).

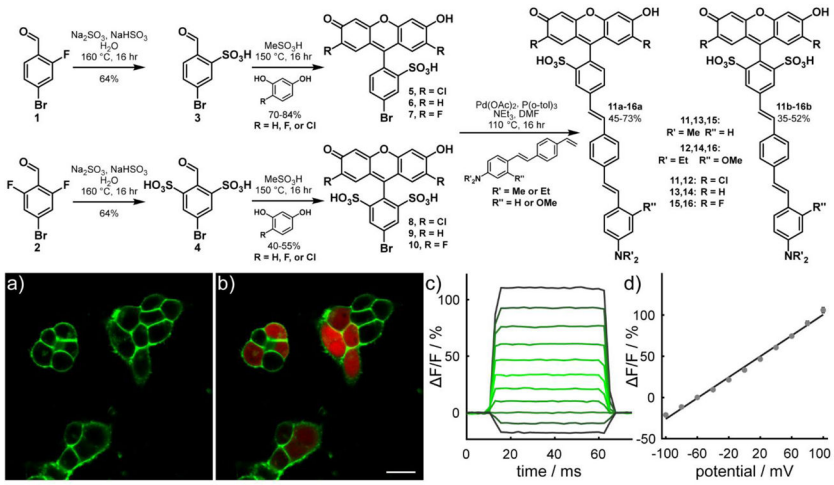

Figure 3.

Synthesis and characterization of monosulfo and disulfoVF dyes. Upper panel: Synthesis of VF dyes. Lower panel: a) Confocal fluorescence images of dsVF2.2(OMe).Cl in HEK cells. Membrane-associated green fluorescence (panel a) shows clear membrane localization when compared with cytosolic mCherry (red, panel b). Scale bar is 20 μm. Membrane-localized dsVF2.2(OMe).Cl is voltage sensitive. c) The fractional change in fluorescence is plotted vs. time for 100 ms hyper- and depolarizing steps (±100 mV, 20 mV increments) from a holding potential of −60 mV for a single HEK cells under whole-cell voltage-clamp mode. d) A plot of % ΔF/F vs. final membrane potential (mV), summarizing data from 8 separate cells, reveals a voltage sensitivity of approximately 63% per 100 mV (±1.6%). Error bars are ±SEM.

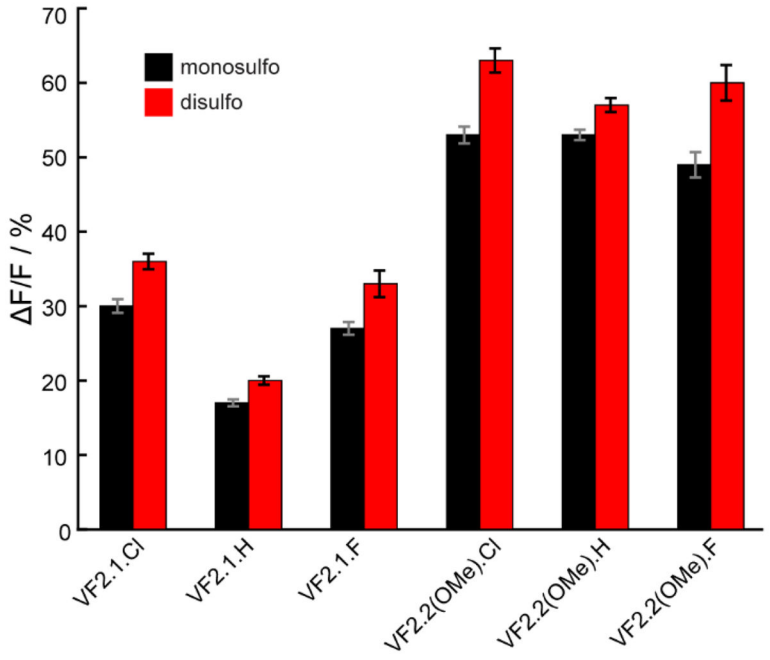

Figure 4.

Comparison of voltage sensitivity of monosulfo- and disulfo-VoltageFluor. Black bars represent msVF dyes and red bars represent dsVF dyes. Voltage sensitivity is reported as ΔF/F per 100 mV as measured in patch-clamped HEK cells. Values represent 3–8 independent determinations and error bars are ±SEM

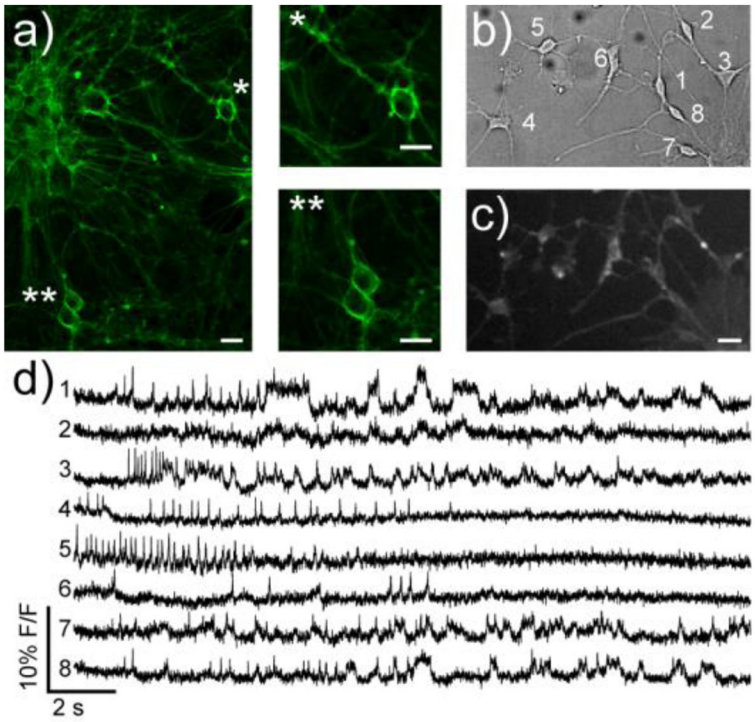

Figure 5.

Imaging membrane potential changes in cultured rat hippocampal neurons and hPSC-derived midbrain dopaminergic (mDA) neurons using dsVF2.2(OMe).Cl. a) Confocal images of rat hippocampal neurons stained with 500 nM dsVF2.2(OMe).Cl. * and ** are zoomed regions of the indicated neurons b) Transmitted light image (DIC) of hPSC-derived mDA neurons. c) Wide field fluorescence image of mDA neurons from panel b stained with 500 nM dsVF2.2(OMe).Cl. d) Fractional change in fluroescence vs. time for cells indicated in panels b. Each trace represents the fluorescence intensity from the indicated cell; all traces have been bleach corrected and are unfiltered. Scale bars are 20 μm.

Table 1

Properties of mono- and disulfo VoltageFluor dyes

Name	ID	R	R′	R″	Φ_{fl}[a]	λ_{abs}[a]	λ_{em}[a]	ΔF/F (%)[b]	Improvement (%)[c]
msVF2.1.Cl	11a	Cl	Me	H	0.06	522	536	30	---
dsVF2.1.Cl	11b	Cl	Me	H	0.08	520	539	36	21
msVF2.2(OMe).Cl	12a	Cl	Et	OMe	0.06	518	534	53	---
dsVF2.2(OMe).Cl	12b	Cl	Et	OMe	0.07	520	540	63	19
msVF2.1.H	13a	H	Me	H	0.10	507	528	17	---
dsVF2.1.H	13b	H	Me	H	0.14	509	540	20	17
msVF2.2(OMe).H	14a	H	Et	OMe	0.08	508	530	53	---
dsVF2.2(OMe).H	14b	H	Et	OMe	0.11	510	530	57	9
msVF2.1.F	15a	F	Me	H	0.09	508	524	27	---
dsVF2.1.F	15b	F	Me	H	0.13	507	529	33	25
msVF2.2(OMe).F	16a	F	Et	OMe	0.06	505	524	49	---
dsVF2.2(OMe).F	16b	F	Et	OMe	0.06	509	529	60	22

[a] Measured in phosphate-buffered saline, pH 7.4 with 0.1% Triton X-100.

[b] per 100 mV. Determined in HEK cells.

[c] Relative to corresponding msVF.